

## **A wake-promoting circadian output circuit in *Drosophila***

Angélique Lamaze<sup>1\*</sup>, Patrick Krätschmer<sup>1,2</sup>, Ko-Fan Chen<sup>1,2</sup>, Simon Lowe<sup>1</sup>,  
and James E. C. Jepson<sup>1,3\*</sup>

<sup>1</sup>Department of Experimental and Clinical Epilepsy, UCL Institute of  
Neurology, London WC1N 3BG, UK

<sup>2</sup>These authors contributed equally to this work

<sup>3</sup>Lead Contact

\*Correspondence: [angie0203@hotmail.com](mailto:angie0203@hotmail.com) (A.L), [j.jepson@ucl.ac.uk](mailto:j.jepson@ucl.ac.uk)  
(J.E.C.J)

## **SUMMARY**

Circadian clocks play conserved roles in gating sleep/wake states throughout the day-night cycle [1-5]. In the fruit fly *Drosophila melanogaster*, DN1p clock neurons have been reported to play both wake- and sleep-promoting roles [6-11], suggesting a complex coupling of DN1p neurons to downstream sleep/arousal centers. However, the circuit logic by which DN1p neurons modulate sleep remains poorly understood. Here we show that DN1p neurons can be divided into two morphologically distinct subsets. Projections from one subset surround the pars intercerebralis, a previously defined circadian output region [12]. In contrast, the second subset also sends presynaptic termini to a visual processing center, the anterior optic tubercle (AOTU) [13]. Within the AOTU, we find that DN1p neurons inhibit a class of tubercular-bulbar (TuBu) neurons that act to promote consolidated sleep. These TuBu neurons in turn form synaptic connections with R-neurons of the ellipsoid body, a region linked to visual feature detection, locomotion, spatial memory, and sleep homeostasis [14-17]. Our results define a second output arm from DN1p neurons and suggest a role for TuBu neurons as regulators of sleep drive.

## RESULTS

### A subset of DN1p neurons innervate the Anterior Optic Tubercle

DN1p neurons can be labelled using either the *clk4.1M*- or *R18H11*-Gal4 drivers, which express in 8-10 and 7-8 DN1p neurons per hemisphere respectively [6, 8]. Since circuits downstream of these neurons are poorly defined, we sought to characterize neuropil regions innervated by DN1p neurons at the single-cell level. To do so, we induced stochastic FLP-mediated removal of an FRT-flanked stop codon upstream of a membrane-tagged GFP coding sequence, driven by either *clk4.1M*- or *R18H11*-Gal4 (Figure 1A, B) [18]. Using this approach, we identified 14 and 12 individual *clk4.1M*- and *R18H11*-positive DN1p neurons respectively. In each case we examined their projection patterns by confocal microscopy and confirmed their clock neuron identity by testing for somatic expression of the clock protein PERIOD (Figure 1C, D).

We identified two morphologically distinct subtypes of DN1p neurons. The first (5/14 *clk4.1M*- and 6/12 *R18H11*-positive DN1p neurons) was characterized by projections that formed a loop-like structure around the superior lateral protocerebrum and innervated the Anterior Optic Tubercle (AOTU) (Figure 1C, D – left panels). At the population level, such structures could be clearly observed in dorsal views of *R18H11*-positive DN1p neurons (Figure 1E, arrows). These neurons also sent projections to posterior neuropil regions that terminated prior to the midline or crossed the midline into the corresponding contralateral domain, close to the pars intercerebralis (PI) (Figure 1C, D and Figure S1A). The second subpopulation (9/14 *clk4.1M*- and 6/12 *R18H11*-positive DN1p neurons) lacked projections to the AOTU.

Instead, they solely extended ventral and contralateral projections confined to posterior regions of the *Drosophila* brain (Figure 1C, D – right panels).

Contralateral projections from this subtype also terminated in close proximity to the PI. We term these two subtypes anterior- and ventro-contralateral-projecting DN1p neurons (a-DN1p and vc-DN1p neurons) respectively.

Excitability of DN1p neurons peaks in the late night/early morning [19, 20], with multiple lines of evidence supporting a wake-promoting role for DN1p neurons during these times [6-9, 19]. Recent work has also suggested that DN1p neurons are sleep-promoting towards the late evening and early night [11]. The same authors subsequently mapped this sleep-promoting effect to 5-6 glutamatergic DN1p neurons labelled using the split-Gal4 system, terming these neurons spl-gDN1 neurons [10, 21]. We wondered whether spl-gDN1 neurons might correspond to one of the a-DN1p and vc-DN1p subpopulations. We therefore expressed membrane-tagged tdTomato using the same DN1 split-Gal4, observing fluorescence in DN1p neurons as well as other neurons and glial cells (Figure S1B). spl-gDN1 neurons did not innervate the AOTU, and their collective ventral and contralateral projection patterns were strikingly similar to those of individual vc-DN1p neurons (Figure S1B, C). These results suggest that sleep-promoting spl-gDN1 neurons may correspond to the vc-DN1p subpopulation, and therefore that wake-promoting DN1p neurons may include the a-DN1p subpopulation that project to the AOTU.

### **DN1p neurons form synaptic contacts with tubercular-bulbar neurons**

To define pre- and post-synaptic sites within neuropil regions innervated by DN1p neurons, we expressed fluorophores localised to presynaptic and

dendritic domains (UAS-*syt-GFP* and UAS-*DenMark* respectively) using *R18H11-Gal4* (Figure 2A-C). Within the dorsal and ventral posterior neuropil we observed presynaptic and dendritic signatures of DN1p neurons (Figure 2A). In contrast, within the AOTU we solely observed presynaptic *syt-GFP* puncta (Figure 2B, C). The AOTU can be subdivided into medial, intermediate medial, intermediate lateral and lateral regions [13] (Figure 2B). Presynaptic termini from a-DN1p neurons predominantly innervated the dorsal-most segment of the intermediate lateral region (AOTUil) (Figure 2B). Similar localisation of a-DN1p synapses was observed when driving *syt-GFP* with *clk4.1M-Gal4* (Figure S2A), confirming that these derive from DN1p neurons.

Within the AOTU, tubercular-bulbar (TuBu) neurons receive visual input from medullo-tubercular neurons and transmit this information to Ellipsoid Body (EB) ring (R-) neurons in the bulb (also known as the lateral triangle) [13, 22, 23]. Given their dendritic innervation of the AOTU, TuBu neurons thus represent candidate cell-types acting downstream of DN1p neurons. To examine this, we identified TuBu neurons with dendrites in the AOTUil using the *R92H07-Gal4* driver (Figure 2D). We used orthogonal LexA- and Gal4-drivers to express different fluorophores in DN1p and *R92H07-TuBu* neurons, revealing close association within the AOTUil (Figure 2D). We also performed GFP reconstitution across synapses (GRASP) by expressing complementary fragments of GFP in DN1p and *R92H07-TuBu* neurons [24]. Confocal imaging revealed reconstituted GFP fluorescence specifically in the dorsal domain of the AOTUil (Figure 2E and Figure S2B). This fluorescence was absent in controls containing single driver lines (Figure 2E), confirming

signal specificity and strongly suggesting that DN1p neurons form synaptic contacts with TuBu neurons.

We also tested whether DN1p neurons formed connections with TuBu neurons in the lateral region of the AOTU (AOTUla). Using the *R83H09*-Gal4 driver, we co-labelled TuBu neurons with dendrites innervating the AOTUla alongside DN1p neurons (Figure S2C). DN1p synapses/axons tiled the boundary of *R83H09*-Tubu dendrites (Figure S2C). However, in contrast to *R92H07*-Tubu neurons, no GRASP signal between DN1p and *R83H09*-Tubu neurons was observed (Figure S2D). Thus, DN1p neurons appear to physically associate predominantly with TuBu neurons in the AOTUil region.

### **DN1p neurons inhibit *R92H07*-TuBu neurons**

We next examined whether DN1p and *R92H07*-TuBu neurons are functionally connected using CaMPARI. When stimulated with UV light, the CaMPARI fluorophore undergoes green-to-red photo-conversion in high intracellular calcium, yielding an optical read-out of neuronal activity [25]. We simultaneously expressed CaMPARI in *R92H07*-TuBu neurons and a temperature-sensitive inhibitor of endocytosis (*sh[ts]*) in DN1p neurons using the *R18H11*-LexA driver. Expression of *sh[ts]* inhibits synaptic vesicle recycling at 31°C but not 22°C, facilitating acute inhibition of DN1p output [26]. Using this protocol, we found that inhibition of *R18H11*-DN1p neurons resulted in a significant increase in CaMPARI photo-conversion in a subset of *R92H07*-TuBu neurons (Figure 3A, B). This partial penetrance is consistent with the additional presence of *R92H07*-TuBu dendrites in the ventral domain of the AOTUil (Fig. 2D), which is not innervated by DN1p synapses (Fig. 2B,

E). In contrast, in the absence of the *R18H11*-LexA driver, shifts from 22°C to 31°C alone did not alter CaMPARI photo-conversion (Figure 3B). Conversely, acute excitation of DN1p neurons using ChannelRhodopsin 2-XXL reduced intracellular calcium levels in *R92H07*-TuBu neurons, as measured using GCaMP6s (Figure S3A, B) [27, 28]. Thus, DN1p neurons suppress excitability of *R92H07*-TuBu neurons.

### ***R92H07*-neurons promote consolidated sleep**

We next examined whether *R92H07*-TuBu neurons modulate sleep/wake patterns. To do so, we expressed TrpA1 (a temperature-gated cation channel) in *R92H07*-neurons and measured sleep following a shift from 22°C (a non-activating temperature) to 31°C (an activating temperature) [29], using the standard definition of a *Drosophila* sleep bout as a 5 min period of inactivity [30]. Using the *Drosophila* Activity Monitor (DAM) system [30], we found that at 22°C, expression of TrpA1 in *R92H07*-neurons had no significant effect on day or night sleep (Figure 3C, D). In contrast, thermo-genetic excitation of *R92H07*-neurons at 31°C profoundly induced sleep throughout both the day and the night compared to controls (Figure 3C, D). On the following day at 22°C, prior *R92H07*-TuBu excitation resulted in a strong 'negative rebound' characterized by reduced day and night sleep relative to controls (Figure 3C, D). These results suggest that *R92H07*-TuBu neurons are sleep-promoting and coupled to circuits that control homeostatic sleep drive, in contrast to other sleep-modulatory cell-types in the fly brain such as octopaminergic neurons [31].

To confirm that these phenotypes were not artefacts caused by temporary paralysis, we monitored locomotor velocities using a video-tracking system (DART: *Drosophila* Arousal Tracking), and applied mechanical stimuli consisting of ten 50 Hz vibrations lasting 1 s, separated by intervals of 500 ms [32]. As expected, excitation of *R92H07*-neurons strongly reduced spontaneous waking locomotor velocities (Figure S3C-E). However, robust responses to vibration stimuli were still observed that were similar in magnitude compared to controls (Figure S3C-G). Thus, *R92H07*-neuron activation does not cause paralysis. Interestingly, locomotor velocities after vibration-induced activity decayed significantly more rapidly when *R92H07*-neurons were activated, consistent with increased sleep drive following brief awakenings (Figure S3F, H).

To test whether suppressing *R92H07*-neuron output impacted sleep, we acutely blocked synaptic release from *R92H07*-neurons using *sh[ts]* (Figure S4A-C). The effect of acute inhibition *R92H07*-neurons on sleep architecture was subtle compared to acute activation (Figure S4B, C and Figure 3C). Nonetheless, the duration of consolidated sleep during the day appeared to be reduced following *R92H07*-neuron inhibition (Figure S4C).

To investigate this in more detail, we generated an R-based program capable of quantifying up to 30 distinct sleep parameters from DAM system data (see STAR Methods), allowing us to measure the duration of *longest* sleep bouts (LSB) during either the day (dLSB) or night (nLSB). LSB onset is clock regulated, with dLSB onset advanced in clock mutants with short circadian periods (*per<sup>S</sup>*) and delayed in mutants with long periods (*per<sup>L</sup>*) [33] (Figure S4D). Furthermore, LSB duration strongly correlates with average

sleep bout duration during the day or night in control flies (Figure S4E, F). Given the often-fragmented nature of *Drosophila* sleep at both low and high temperatures (Figure S4G, H), measuring LSB onset and duration yields a more accurate description of the dynamics of consolidated sleep. We therefore measured dLSB and nLSB duration following acute inhibition of *R92H07*-neurons. At the non-inhibiting temperature of 22°C, expression of *sh[ts]* in *R92H07*-neurons did not alter dLSB or nLSB duration (Figure S4I, J). In contrast, at the inhibiting temperature of 31°C, expression of *sh[ts]* in *R92H07*-neurons resulted in a significant reduction in the duration of the dLSB but not the nLSB (Figure S4K, L). *R92H07*-neurons may thus promote consolidated sleep patterns predominantly during the light phase of the day, consistent with excitation of TuBu neurons by visual projection neurons [13].

### **Sleep-regulatory TuBu neurons form synaptic connections with R-neurons**

Finally, we sought to identify circuits downstream of *R92H07*-TuBu neurons. Initially, we used a recently devised system for unbiased trans-synaptic labelling: *trans*-Tango [34]. Via an engineered signalling pathway, *trans*-Tango induces simultaneous myr-GFP expression in defined pre-synaptic neurons and mtdTomato expression in their post-synaptic partners. When *trans*-Tango was driven by *R92H07*-Gal4, we observed overlapping myr-GFP and mtdTomato fluorescence in the superior bulb that was absent in controls lacking the *R92H07*-Gal4 driver (Figure 4A) [13]. Neurons post-synaptic to *R92H07*-TuBu neurons projected to the EB ring (Figure 4A, right panel), consistent with recent studies demonstrating feed-forward connectivity

between TuBu and EB ring- (R-) neurons [13, 22, 23]. From the location of their dendrites in the superior bulb and axonal projections in the outer segments of the EB, these R-neurons may comprise the R2-, R4d- R5- subtypes (Figure 4A) [13, 22].

To examine this in more detail, we used orthogonal expression systems to label both *R92H07*-TuBu neurons and distinct R-neurons. Within the  $Bu_s$ , *R92H07*-TuBu axons did not overlap with dendrites of R4d-neurons labelled using *R40D05*-Gal4 (Figure 4B, upper panel), where R4d-neurons are defined by dendrites innervating the superior bulb and axons tilling the outmost region of the EB ring [22]. R2- and R4m-neurons can be labelled using the *R20D01*-Gal4 driver [35]. These subtypes can be distinguished by their differential dendritic innervation of the  $Bu_s$  (R2) and inferior bulb (R4m), which are dorso-lateral and lateral to the EB midline respectively [13]. We found that a subset of *R92H07*-TuBu neuron synaptic termini overlapped with R2 dendrites (Figure 4B, middle and lower panels), and confirmed synaptic connectivity between *R92H07*-TuBu and R2-neurons in superior bulb using GRASP (Figure 4C). Collectively, our results suggest that DN1p clock neurons and EB R2-neurons are functionally connected via *R92H07*-TuBu neurons (Figure 4D).

## **DISCUSSION**

Previous work has shown that DN1p clock neurons signal to the pars intercerebralis as part of a pathway regulating circadian locomotor rhythms [12]. By analysing morphological diversity of DN1p neurons we identify a second output circuit linking DN1p neurons to EB R2-neurons via sleep-promoting TuBu neurons. Consistent with our finding that *R92H07*-TuBu

neurons promote sleep drive, recent studies have suggested a role for R2-neurons as components of *Drosophila* sleep homeostat circuitry [14, 36]. However, these are likely to be distinct from the R2-neurons described here, as separate classifications of R-neuron subtypes exist in prior literature. We follow recent anatomical characterizations and define R2-neurons as possessing dendrites within the superior bulb, axonal bundles that enter the EB at its midline, and columnar axons within the EB ring [13, 22]. In contrast, axons from sleep-regulatory ring neurons also described as R2-neurons enter the EB at dorso-ventral points and do not possess columnar axons [14, 36], thus corresponding to R5-neurons as defined by other groups [13, 22]. However, since both *R92H07*-TuBu synapses and R5 dendrites are present in the superior bulb, and only a subset of *R92H07*-TuBu neuron synapses overlap with R2 dendrites (Figure 4B), communication between *R92H07*-TuBu neurons and R5-neurons remains a possibility. Indeed, we hypothesize that *R92H07*-TuBu neurons may regulate sleep via simultaneous input to multiple R-neuron subtypes.

In *Drosophila*, R2-neurons play roles in visual feature detection, pattern memory and decision-making [15, 37, 38]. Thus, in addition to regulating the timing of consolidated sleep, the circuit we have identified may provide a pathway for circadian modulation of several ethologically relevant behaviors. It is also intriguing to speculate about potential roles in other insect species. TuBu neurons receive visual input from medullo-tubercular (MeTu) neurons, with the tripartite MeTu > TuBu > R-neuron circuit known as the anterior visual pathway (AVP). The *Drosophila* AVP is structurally similar to the sky-compass pathway used in honeybees, locusts and butterflies to navigate relative to the

Sun [13, 39]. Circadian input into the sky-compass pathway is required to adjust for changes in the position of the Sun's azimuth across the day [40], yet which clock circuits give time information to the sky compass remains unclear. Since dorsal neurons expressing the PERIOD clock protein are present in a wide range of insect species [41], it will be intriguing to examine whether these DN1p-like neurons intersect with the sky compass pathway and drive circadian changes in feature-dependent orientation.

## **ACKNOWLEDGEMENTS**

We thank Gilad Barnea, Kyunghhee Koh, Francois Rouyer and Ralf Stanewsky for *Drosophila* stocks; and Kyunghhee Koh and Francois Rouyer for helpful comments on the manuscript. This study was supported by a UCL Start-Up Fund to J.E.C.J.

## **AUTHOR CONTRIBUTIONS**

Conceptualization: A.L and J.E.C.J. Methodology: A.L, P.K. K-F.C, S.L, J.E.C.J. Software: P.K. Validation: A.L. Formal Analysis: A.L, P.K, J.E.C.J. Investigation: A.L, P.K. K-F.C, S.L, J.E.C.J. Writing – Original Draft: J.E.C.J and A.L. Writing – Review and Editing: A.L, P.K. K-F.C, S.L, J.E.C.J. Visualisation: A.L, P.K and J.E.C.J. Supervision: J.E.C.J. Project Administration: J.E.C.J. Funding Acquisition: J.E.C.J.

## **DECLARATION OF INTERESTS**

The authors declare no competing interests.

## REFERENCES

1. Aston-Jones, G., Chen, S., Zhu, Y., and Oshinsky, M.L. (2001). A neural circuit for circadian regulation of arousal. *Nat Neurosci* 4, 732-738.
2. Chou, T.C., Scammell, T.E., Gooley, J.J., Gaus, S.E., Saper, C.B., and Lu, J. (2003). Critical role of dorsomedial hypothalamic nucleus in a wide range of behavioral circadian rhythms. *J Neurosci* 23, 10691-10702.
3. Wurts, S.W., and Edgar, D.M. (2000). Circadian and homeostatic control of rapid eye movement (REM) sleep: promotion of REM tendency by the suprachiasmatic nucleus. *J Neurosci* 20, 4300-4310.
4. Liu, S., Lamaze, A., Liu, Q., Tabuchi, M., Yang, Y., Fowler, M., Bharadwaj, R., Zhang, J., Bedont, J., Blackshaw, S., et al. (2014). WIDE AWAKE mediates the circadian timing of sleep onset. *Neuron* 82, 151-166.
5. Toh, K.L., Jones, C.R., He, Y., Eide, E.J., Hinz, W.A., Virshup, D.M., Ptacek, L.J., and Fu, Y.H. (2001). An hPer2 phosphorylation site mutation in familial advanced sleep phase syndrome. *Science* 291, 1040-1043.
6. Kunst, M., Hughes, M.E., Raccuglia, D., Felix, M., Li, M., Barnett, G., Duah, J., and Nitabach, M.N. (2014). Calcitonin gene-related peptide neurons mediate sleep-specific circadian output in *Drosophila*. *Curr Biol* 24, 2652-2664.
7. Lamaze, A., Ozturk-Colak, A., Fischer, R., Peschel, N., Koh, K., and Jepson, J.E. (2017). Regulation of sleep plasticity by a thermo-sensitive circuit in *Drosophila*. *Sci Rep* 7, 40304.
8. Zhang, L., Chung, B.Y., Lear, B.C., Kilman, V.L., Liu, Y., Mahesh, G., Meissner, R.A., Hardin, P.E., and Allada, R. (2010). DN1(p) circadian neurons coordinate acute light and PDF inputs to produce robust daily behavior in *Drosophila*. *Curr Biol* 20, 591-599.
9. Zhang, Y., Liu, Y., Bilodeau-Wentworth, D., Hardin, P.E., and Emery, P. (2010). Light and temperature control the contribution of specific DN1 neurons to *Drosophila* circadian behavior. *Curr Biol* 20, 600-605.
10. Guo, F., Chen, X., and Rosbash, M. (2017). Temporal calcium profiling of specific circadian neurons in freely moving flies. *Proc Natl Acad Sci U S A* 114, E8780-E8787.
11. Guo, F., Yu, J., Jung, H.J., Abruzzi, K.C., Luo, W., Griffith, L.C., and Rosbash, M. (2016). Circadian neuron feedback controls the *Drosophila* sleep--activity profile. *Nature* 536, 292-297.
12. Cavanaugh, D.J., Geratowski, J.D., Wooltorton, J.R., Spaethling, J.M., Hector, C.E., Zheng, X., Johnson, E.C., Eberwine, J.H., and Sehgal, A. (2014). Identification of a circadian output circuit for rest:activity rhythms in *Drosophila*. *Cell* 157, 689-701.
13. Omoto, J.J., Keles, M.F., Nguyen, B.M., Bolanos, C., Lovick, J.K., Frye, M.A., and Hartenstein, V. (2017). Visual Input to the *Drosophila* Central Complex by Developmentally and Functionally Distinct Neuronal Populations. *Curr Biol* 27, 1098-1110.
14. Liu, S., Liu, Q., Tabuchi, M., and Wu, M.N. (2016). Sleep Drive Is Encoded by Neural Plastic Changes in a Dedicated Circuit. *Cell* 165, 1347-1360.

15. Seelig, J.D., and Jayaraman, V. (2013). Feature detection and orientation tuning in the *Drosophila* central complex. *Nature* 503, 262-266.
16. Ilius, M., Wolf, R., and Heisenberg, M. (1994). The central complex of *Drosophila melanogaster* is involved in flight control: studies on mutants and mosaics of the gene ellipsoid body open. *J Neurogenet* 9, 189-206.
17. Neuser, K., Triphan, T., Mronz, M., Poeck, B., and Strauss, R. (2008). Analysis of a spatial orientation memory in *Drosophila*. *Nature* 453, 1244-1247.
18. Yu, J.Y., Kanai, M.I., Demir, E., Jefferis, G.S., and Dickson, B.J. (2010). Cellular organization of the neural circuit that drives *Drosophila* courtship behavior. *Curr Biol* 20, 1602-1614.
19. Flourakis, M., Kula-Eversole, E., Hutchison, A.L., Han, T.H., Aranda, K., Moose, D.L., White, K.P., Dinner, A.R., Lear, B.C., Ren, D., et al. (2015). A Conserved Bicycle Model for Circadian Clock Control of Membrane Excitability. *Cell* 162, 836-848.
20. Liang, X., Holy, T.E., and Taghert, P.H. (2016). Synchronous *Drosophila* circadian pacemakers display nonsynchronous Ca(2)(+) rhythms in vivo. *Science* 351, 976-981.
21. Luan, H., Peabody, N.C., Vinson, C.R., and White, B.H. (2006). Refined spatial manipulation of neuronal function by combinatorial restriction of transgene expression. *Neuron* 52, 425-436.
22. Timaeus, L., Geid, L., and Hummel, T. (2018). A topographic visual pathway into the central brain of *Drosophila*. *bioRxiv* <https://www.biorxiv.org/content/early/2017/09/05/183707>.
23. Sun, Y., Nern, A., Franconville, R., Dana, H., Schreiter, E.R., Looger, L.L., Svoboda, K., Kim, D.S., Hermundstad, A.M., and Jayaraman, V. (2017). Neural signatures of dynamic stimulus selection in *Drosophila*. *Nat Neurosci* 20, 1104-1113.
24. Feinberg, E.H., Vanhoven, M.K., Bendesky, A., Wang, G., Fetter, R.D., Shen, K., and Bargmann, C.I. (2008). GFP Reconstitution Across Synaptic Partners (GRASP) defines cell contacts and synapses in living nervous systems. *Neuron* 57, 353-363.
25. Fosque, B.F., Sun, Y., Dana, H., Yang, C.T., Ohyama, T., Tadross, M.R., Patel, R., Zlatic, M., Kim, D.S., Ahrens, M.B., et al. (2015). Neural circuits. Labeling of active neural circuits in vivo with designed calcium integrators. *Science* 347, 755-760.
26. Kitamoto, T. (2001). Conditional modification of behavior in *Drosophila* by targeted expression of a temperature-sensitive shibire allele in defined neurons. *J Neurobiol* 47, 81-92.
27. Chen, T.W., Wardill, T.J., Sun, Y., Pulver, S.R., Renninger, S.L., Baohan, A., Schreiter, E.R., Kerr, R.A., Orger, M.B., Jayaraman, V., et al. (2013). Ultrasensitive fluorescent proteins for imaging neuronal activity. *Nature* 499, 295-300.
28. Dawydow, A., Gueta, R., Ljaschenko, D., Ullrich, S., Hermann, M., Ehmann, N., Gao, S., Fiala, A., Langenhan, T., Nagel, G., et al. (2014). Channelrhodopsin-2-XXL, a powerful optogenetic tool for low-light applications. *Proc Natl Acad Sci U S A* 111, 13972-13977.

29. Hamada, F.N., Rosenzweig, M., Kang, K., Pulver, S.R., Ghezzi, A., Jegla, T.J., and Garrity, P.A. (2008). An internal thermal sensor controlling temperature preference in *Drosophila*. *Nature* *454*, 217-220.
30. Pfeiffenberger, C., Lear, B.C., Keegan, K.P., and Allada, R. (2010). Processing sleep data created with the *Drosophila* Activity Monitoring (DAM) System. *Cold Spring Harb Protoc* *2010*, pdb prot5520.
31. Seidner, G., Robinson, J.E., Wu, M., Worden, K., Masek, P., Roberts, S.W., Keene, A.C., and Joiner, W.J. (2015). Identification of Neurons with a Privileged Role in Sleep Homeostasis in *Drosophila melanogaster*. *Curr Biol* *25*, 2928-2938.
32. Faville, R., Kottler, B., Goodhill, G.J., Shaw, P.J., and van Swinderen, B. (2015). How deeply does your mutant sleep? Probing arousal to better understand sleep defects in *Drosophila*. *Sci Rep* *5*, 8454.
33. Konopka, R.J., and Benzer, S. (1971). Clock mutants of *Drosophila melanogaster*. *Proc Natl Acad Sci U S A* *68*, 2112-2116.
34. Talay, M., Richman, E.B., Snell, N.J., Hartmann, G.G., Fisher, J.D., Sorkac, A., Santoyo, J.F., Chou-Freed, C., Nair, N., Johnson, M., et al. (2017). Transsynaptic Mapping of Second-Order Taste Neurons in Flies by trans-Tango. *Neuron* *96*, 783-795 e784.
35. Xie, X., Tabuchi, M., Brown, M.P., Mitchell, S.P., Wu, M.N., and Kolodkin, A.L. (2017). The laminar organization of the *Drosophila* ellipsoid body is semaphorin-dependent and prevents the formation of ectopic synaptic connections. *Elife* *6*.
36. Donlea, J.M., Pimentel, D., Talbot, C.B., Kempf, A., Omoto, J.J., Hartenstein, V., and Miesenbock, G. (2018). Recurrent Circuitry for Balancing Sleep Need and Sleep. *Neuron*.
37. Azanchi, R., Kaun, K.R., and Heberlein, U. (2013). Competing dopamine neurons drive oviposition choice for ethanol in *Drosophila*. *Proc Natl Acad Sci U S A* *110*, 21153-21158.
38. Pan, Y., Zhou, Y., Guo, C., Gong, H., Gong, Z., and Liu, L. (2009). Differential roles of the fan-shaped body and the ellipsoid body in *Drosophila* visual pattern memory. *Learn Mem* *16*, 289-295.
39. Homberg, U. (2004). In search of the sky compass in the insect brain. *Naturwissenschaften* *91*, 199-208.
40. Lindauer, M. (1960). Time-compensated sun orientation in bees. *Cold Spring Harb Symp Quant Biol* *25*, 371-377.
41. Helfrich-Forster, C., Nitabach, M.N., and Holmes, T.C. (2011). Insect circadian clock outputs. *Essays Biochem* *49*, 87-101.
42. Gordon, M.D., and Scott, K. (2009). Motor control in a *Drosophila* taste circuit. *Neuron* *61*, 373-384.
43. Wu, J.S., and Luo, L. (2006). A protocol for dissecting *Drosophila melanogaster* brains for live imaging or immunostaining. *Nat Protoc* *1*, 2110-2115.
44. Shafer, O.T., Helfrich-Forster, C., Renn, S.C., and Taghert, P.H. (2006). Reevaluation of *Drosophila melanogaster's* neuronal circadian pacemakers reveals new neuronal classes. *J Comp Neurol* *498*, 180-193.

## FIGURE LEGENDS

### Figure 1: Projections from a subset of DN1p neurons terminate in the AOTU.

(A-B) Strategy to label individual DN1p neurons. When driven by the DN1p drivers *clk4.1M*- or *R18H11*-Gal4, expression of a *FRT-stop-FRT-CD8::GFP* transgene does not yield CD8::GFP due to the 5' stop codon (A). Heat-shock-activated FLP expression induces stochastic removal of the FRT-flanked stop codon-containing sequence, and thus CD8::GFP expression (B).

(C-D) Representative examples of a-DN1p and vc-DN1p neurons labelled with *clk4.1M*-Gal4 (C) or *R18H11*-Gal4 (D). Confocal images are shown alongside digital tracings using the simple neurite tracing Image-J plug-in. Note that fine posterior a-DN1p processes are obscured in confocal z-stacks by the intervening neuropil. Arrows: termination sites in the AOTU.

Presynaptic neuropil is labelled using an anti-Bruchpilot (BRP) antibody. Zooms of AOTU regions are shown below. Arrows point to the AOTUil, where CD8::GFP signal from a-DN1p but not vc-DN1p neurons can be observed. PER expression in cell bodies of the a-DN1p and vc-DN1p populations is also shown. Scale bars, 20  $\mu\text{m}$ .

(E) Confocal dorsal z-stack of *R18H11*-positive DN1p projections. Note axonal projections around the lateral superior protocerebrum (filled arrows). Open arrow: innervation site in the AOTU in one hemisphere. Scale bar, 50  $\mu\text{m}$ . See also Figure S1.

**Figure 2. DN1p neurons form synaptic contacts with TuBu neurons in the AOTU.**

(A) Pre-synaptic (left) and dendritic (right) regions of *R18H11*-positive DN1p neurons within the posterior neuropil, labelled by SYT-GFP and DenMark respectively. BRP: presynaptic neuropil.

(B-C) SYT-GFP puncta driven by *R18H11*-Gal4 are observed in the AOTU

(B). Subdomains of the AOTU are as follows. La: lateral, il: intermediate lateral, im: intermediate medial, m: medial [13]. DN1p synapses are predominantly localised to the dorsal compartment of the AOTUil (arrow). In contrast, no DN1p dendrites in the AOTU were observed (C).

(D) Upper panel. Confocal images showing projection patterns of DN1p neurons (labelled using *R18H11*-LexA) and *R92H07*-TuBu neurons. Distinct fluorophores were expressed in DN1p and *R92H07*-TuBu neurons (CD8::GFP and CD4::tdTomato respectively). Arrows: AOTU region. Lower panel: high-resolution image of the AOTU showing overlap (arrows) between DN1p axons and dendrites of *R92H07*-TuBu neurons.

(E) Synaptic connectivity between DN1p and *R92H07*-TuBu neurons, demonstrated by GRASP. Arrows: reconstituted GFP in the dorsal compartment of the AOTUil following expression of membrane-tagged GFP fragments in DN1p and *R92H07*-TuBu neurons (lower panels). This signal was absent in controls containing one of the two driver lines (upper and middle panels). Scale bars: 50  $\mu$ m. See also Figure S2.

**Figure 3. DN1p neurons inhibit sleep-promoting TuBu neurons.**

(A) Confocal images of non-converted (green) and photo-converted (magenta) CaMPARI driven in TuBu neurons by *R92H07*-Gal4. The Fire LUT illustrates changes in CaMPARI photo-conversion. LexAop-*shi*[ts] was simultaneously expressed in DN1p neurons using *R18H11*-LexA. A shift from 22°C to 31°C suppresses DN1p output by activating dominant-negative *shibire*,

(B) DN1p inhibition significantly increases CaMPARI photo-conversion in *R92H07*-TuBu neurons. This is not observed in controls lacking the *R18H11*-LexA driver following an identical temperature shift from 22°C to 31°C.

(C) Overlaid mean sleep levels in adult *Drosophila* males across three consecutive 24 h periods at 22°C (control day), 31°C (TrpA1 activation) and 22°C (recovery day). Error bars, SEM. *R92H07* > +: n = 29; + > *TrpA1*: n = 34; *R92H07* > *TrpA1*: n = 36.

(D) Median sleep levels in the conditions described in (C). Tukey box plots show the 25<sup>th</sup>, median and 75<sup>th</sup> percentiles. Whiskers show 1.5x the interquartile range.

\*\*\*p < 0.0005, ns – p > 0.05, Mann-Whitney U-test (B) or Kruskal-Wallis test with Dunn's post-hoc test (D). See also Figures S3 and S4.

**Figure 4: Ellipsoid body R2-neurons are downstream of sleep-promoting TuBu neurons**

(A) Confocal image of a control *trans*-Tango male adult brain lacking any Gal4 driver (left panel), or *trans*-Tango driven by *R92H07*-Gal4 (middle and right panels). myr-GFP: *R92H07*-TuBu neurons. Projections from a small population of non-TuBu neurons are also labelled at very low levels.

mtdTomato (mtdTom): post-synaptic neurons. Arrows: overlap of myr-GFP and mtdTomato signals in the superior bulb, with projections from downstream neurons innervating the ellipsoid body (EB) rings. Scale bars: 50  $\mu$ m. BRP, Bruchpilot.

(B) Top panel: *R92H07*-TuBu neurons and R4d-neurons defined by *R40D05*-Gal4. No overlap between *R92H07*-TuBu neuron axons and R4d-neuron dendrites was observed in the superior bulb. Middle and lower panels: *R92H07*-TuBu neurons and R2/R4m-neurons defined by *R20D01*-Gal4. The inferior ( $Bu_i$ ) and superior ( $Bu_s$ ) bulbs harbour dendrites of R4m- and R2-neurons respectively. Overlap of a subset of *R92H07*-TuBu axons with R2-neuron dendrites was observed in the  $Bu_s$  (middle panel, arrow), shown in closer magnification in lower panel (arrow). Scale bars: upper and middle panel – 50  $\mu$ m, lower panels – 10  $\mu$ m.

(C) Synaptic connectivity between and *R92H07*-TuBu neurons and R2-neurons confirmed by GRASP. Arrows: reconstituted GFP signal in the region of the  $Bu_s$ , dorso-laterally to the EB midline. GRASP was absent in controls containing single driver lines (upper and middle panels). Scale: 50  $\mu$ m.

(D) Circuit model. Anterior-projecting DN1p (a-DN1p) neurons inhibit sleep-promoting tubercular-bulbar (TuBu) neurons in the AOTU. These relay

information to R-neurons (including R2-neurons) in the superior bulb ( $Bu_s$ ), which innervate the ellipsoid body (EB), a sleep-regulatory neuropil domain.

## **STAR METHODS**

### **CONTACT FOR REAGENT AND RESOURCE SHARING**

Further information and requests for resources and reagents should be directed to and will be fulfilled by the Lead Contact, James Jepson (j.jepson@ucl.ac.uk)

### **EXPERIMENTAL MODEL AND SUBJECT DETAILS**

Fly strains and crosses were reared on standard yeast-containing fly food at a constant temperature of 25°C, housed under 12 h: 12 h light-dark cycles (LD). *Drosophila* lines used for behavioural analysis were outcrossed for a minimum of four generations into an isogenic (*iso31*) background. Individual 2-4 day old males were used in all behavioural experiments. *per<sup>L</sup>* and *per<sup>S</sup>* mutant lines were kind gifts from Francois Rouyer and Ralf Stanewsky. *Trans-Tango* lines were a kind gift from Gilad Barnea.

### **METHOD DETAILS**

#### Behavioral assays

Individual males were loaded into glass tubes containing 2% agar and 4% sucrose. Sleep measurements were performed using either the *Drosophila* Activity Monitor (DAM) system (Trikinetics, MA, USA) [30] or the DART system (BFK Lab, UK) [32]. For all experiments shown in this manuscript, Trikinetics monitors were housed in temperature- and light-controlled incubators (LMS, UK) as described previously [7]. Sleep graphs derived from Trikinetics data and locomotor velocity plots derived from DART data were generated using GraphPad Prism 6.

### Immunohistochemistry

Adult male *Drosophila* brains were immuno-stained as described previously [43]. Brains were fixed in 4% paraformaldehyde at RT for 20 min, and blocked in 5% goat serum at RT for 1 h. Primary antibodies used were as follows: rabbit anti-DsRed (Clontech) – 1:2000; mouse anti-Bruchpilot (nc82, Developmental Studies Hybridoma Bank (DSHB)) – 1:200; chicken anti-GFP (ThermoFisher) – 1:1000; rabbit anti-PER – 1:50000 (kind gift of Ralf Stanewsky). Alexa-fluor secondary antibodies (goat anti-rabbit 555, goat anti-mouse 555, goat anti-chicken 488 and goat anti-mouse 647; ThermoFisher) were used at 1:1-2000 except for labelling anti-BRP with goat anti-mouse 647 or anti-mouse 555, where a dilution of 1:500 was used.

### Mosaic analysis of DN1p clock neurons

To induce expression of a membrane-tagged fluorophore (CD8::GFP) in single DN1p clock neurons, we utilised the *UAS-FRT-stop-FRT-CD8::GFP* transgene in concert with either the *clk4.1M*- or *R18H11*-Gal4 drivers and a *hs-FLP* transgene, which enables heat-induced expression of FLP. Since DN1p neurogenesis occurs during the pupal phase [44], we subjected *clk4.1M* > *UAS-FRT-stop-FRT-CD8::GFP*, *hs-FLP* or *R18H11* > *UAS-FRT-stop-FRT-CD8::GFP*, *hs-FLP* *Drosophila* to 1 h heat-shocks at 37°C on 2-3 consecutive days during the early-late pupal stages. Male offspring of the desired genotypes were subsequently collected post-eclosion, aged for 2-5 days, and dissected at ZT1-3. We used confocal microscopy combined with immuno-

staining to identify male brains containing readily identifiable single DN1p neurons in either hemisphere. For *clk4.1M > UAS-FRT-stop-FRT-CD8::GFP, hs-FLP*, we identified 14 individual DN1p neurons from n = 104 dissected brains. For *R18H11 > UAS-FRT-stop-FRT-CD8::GFP, hs-FLP*, we identified 12 individual DN1p neurons from n = 113 brains. Antibodies against BRP and PERIOD were used to identify the site of DN1p innervation and to confirm that these neurons were bona fide clock neurons.

### Confocal imaging and optogenetics

All optical imaging experiments were performed using an inverted Zeiss LSM 710 confocal microscope. For experiments involving CaMPARI, crosses were performed at 25°C. Subsequently, 1-3 days old flies were entrained in 12 h light: 12 h dark (LD) cycles at 22°C. 48 h prior to the experiment, adult male *Drosophila* were transferred to individual glass tubes to facilitate catching without CO<sub>2</sub> or cold-induced anaesthesia. On the experimental day, individual flies were manually caught and brains were subsequently dissected in HL3.1 buffer, of composition: 70 mM NaCl, 5 mM KCl, 20 mM MgCl<sub>2</sub>, 1.5 mM CaCl<sub>2</sub>, 10 mM NaHCO<sub>3</sub>, 5 mM Trehalose, 115 mM sucrose, 5 mM HEPES, pH 7.2. To induce photo-conversion, UV exposure was undertaken using a high power mercury lamp for 2 min. The more calcium-insensitive V398D variant of CaMPARI was used to increase the dynamic range of photo-conversion [25]. When testing for changes in CaMPARI photo-conversion at 31°C (following DN1p inhibition using *shi[ts]*), the dissection buffer was pre-heated to 31°C in order to maintain the experimental temperature. CaMPARI imaging experiments were

performed at ZT1-3, when DN1p excitability is high [19]. Quantification of CaMPARI photo-conversion in control and experimental TuBu neurons was performed blind with respect to genotype. For experiments involving GCamP6s, brains were also dissected and imaged in HL3.1 buffer. Experiments were performed at ZT9, since average DN1p excitability is low at this time point [19], and at 31°C. Similarly to CaMPARI experiments, dissection buffer was pre-heated to 31°C. To excite GCamP6s, a 514 nm laser was used, whereas to activate ChR2XXL, a 405nm laser was applied.

## **QUANTIFICATION AND STATISTICAL ANALYSIS**

Since many of the datasets derived from sleep experiments exhibited a non-normal distribution, the following statistical tests were used. For single comparisons, Mann-Whitney U-tests were used. When comparing multiple genotypes, Kruskal-Wallis tests were used, followed by Dunn's post-hoc tests. All statistical analyses were performed using GraphPad Prism 6. For each dataset, details of statistical tests used, n-values, dispersion and precision measures can be found in the corresponding Figure Legends.

## **DATA AND SOFTWARE AVAILABILITY**

Detailed documentation of the R program used to analyse the duration, onset and offset of the longest sleep bout, as well as all the corresponding code, can be downloaded or cloned from the following GitHub link:

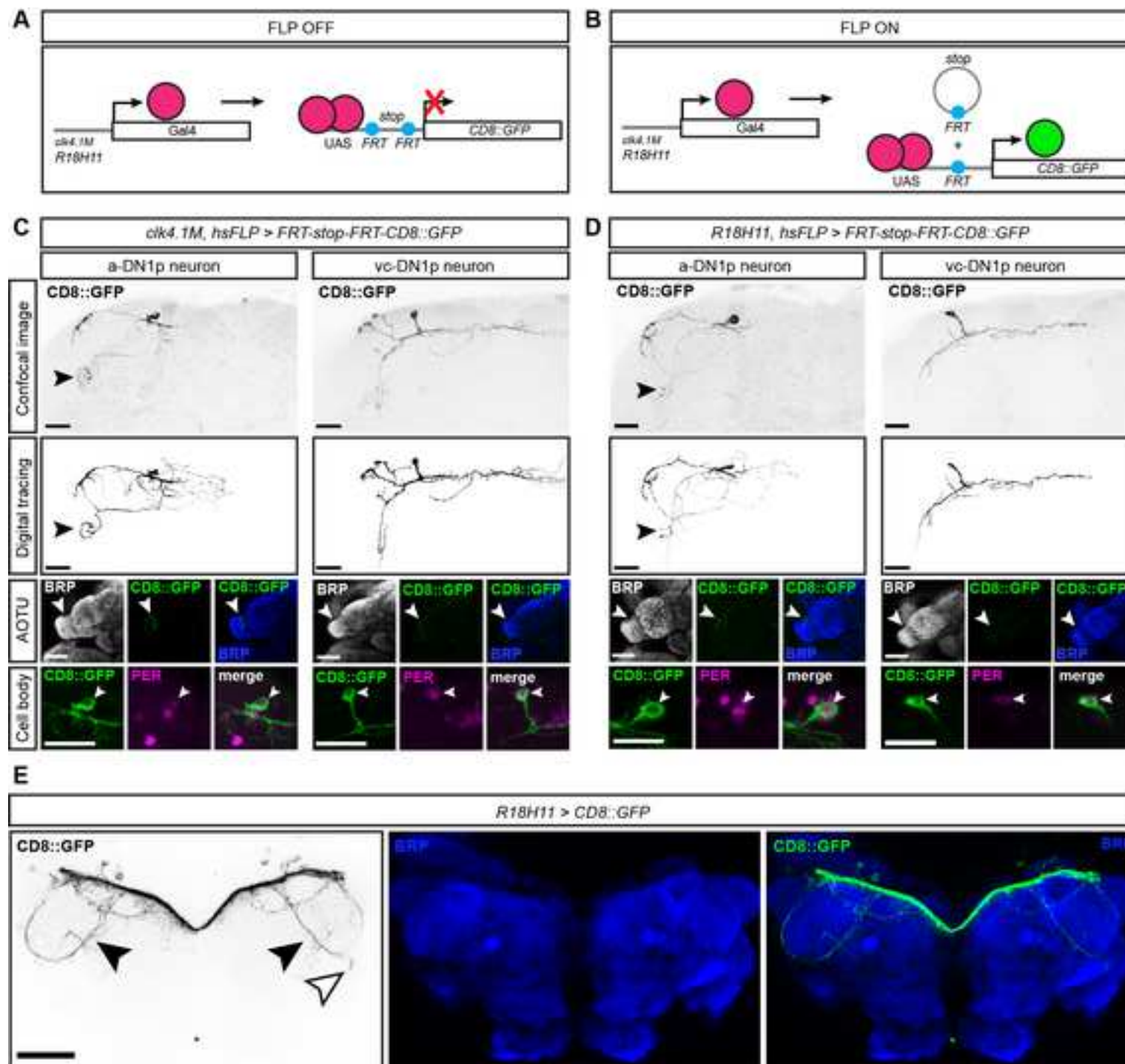
[https://github.com/PatrickKratsch/DAM\\_sleep\\_parameters](https://github.com/PatrickKratsch/DAM_sleep_parameters)

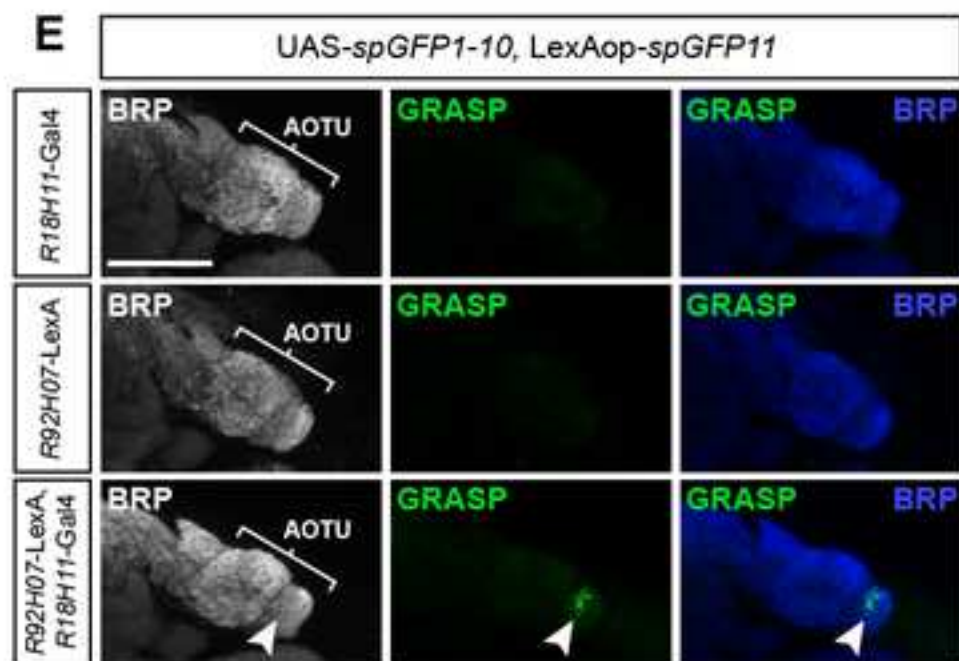
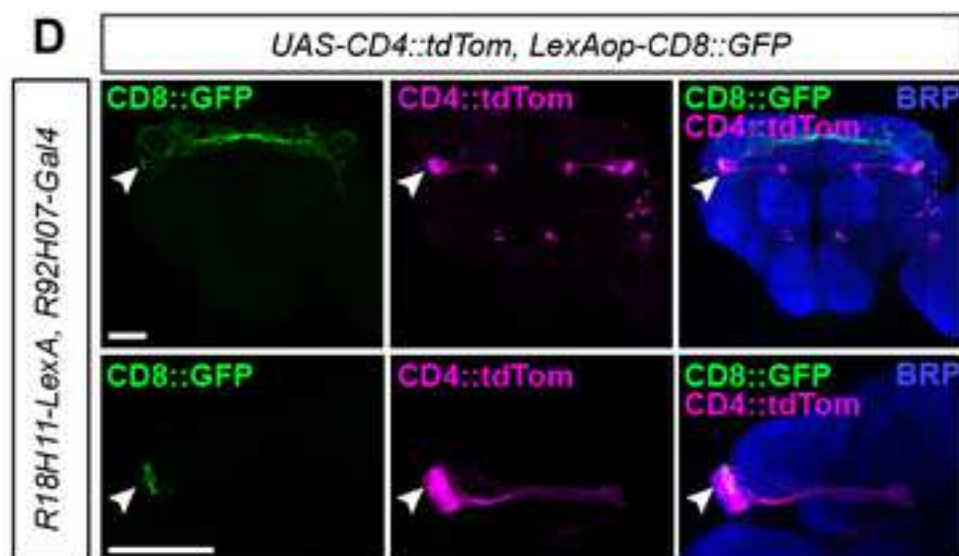
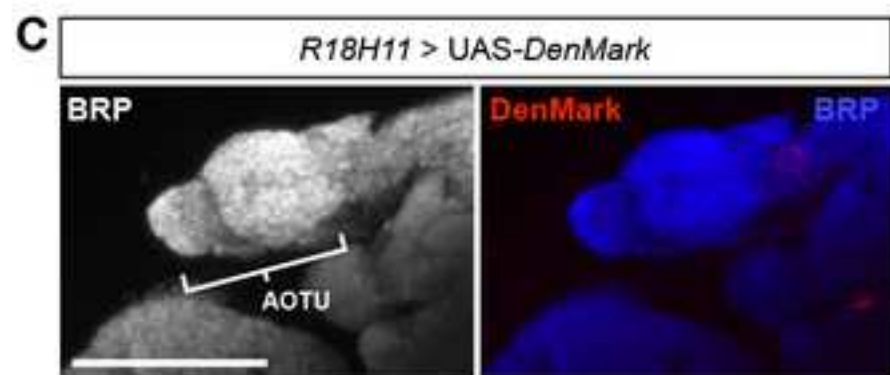
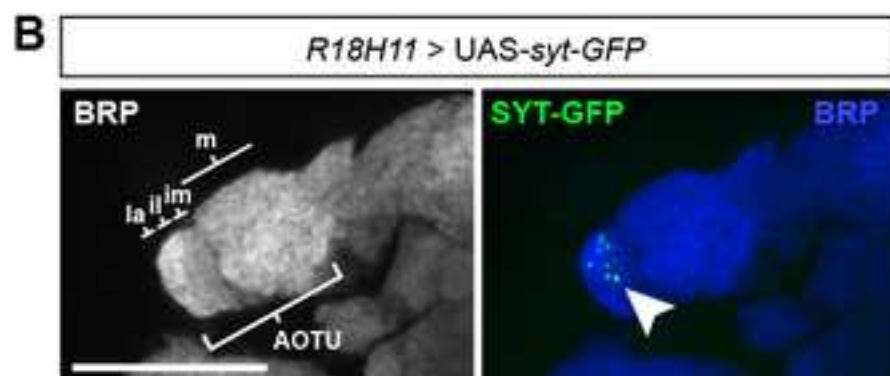
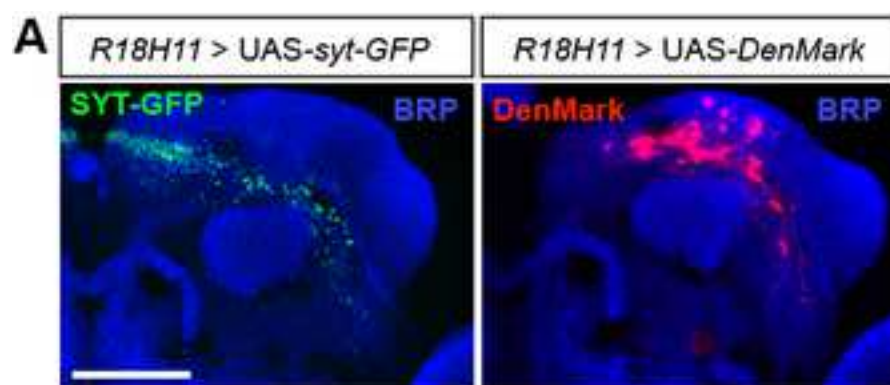
## KEY RESOURCES TABLE

REAGENT or RESOURCE	SOURCE	IDENTIFIER
Antibodies		
Rabbit anti-DsRed	Clontech	Cat#632496
Mouse anti-Bruchpilot	Developmental Studies Hybridoma Bank	nc82
Rabbit anti-PERIOD	Prof. Ralf Stanewsky (University of Muenster)	
Chicken anti-GFP	ThermoFisher	Cat#A10262
Goat anti-Rabbit Alexa Fluor-555	ThermoFisher	Cat#A32732
Goat anti-Chicken Alexa Fluor-488	ThermoFisher	Cat#A11039
Goat anti-Mouse Alexa Fluor-647	ThermoFisher	Cat#A21236
Goat anti-Mouse Alexa Fluor-555	ThermoFisher	Cat#A28180
Chemicals, Peptides, and Recombinant Proteins		
Agar	Sigma-Aldrich	A1296
Sucrose	Calbiochem	5737
4% Paraformaldehyde	Alfa Aesar	43368
Triton X-100	Sigma-Aldrich	X100
Experimental Models: Organisms/Strains		
w[*]; P{w[+mC]=UAS-shi[ts1].K}3	Bloomington Stock Centre (USA)	BL#44222
w[*]; P{y[+7.7] w[+mC]=UAS-TrpA1(B).K}attP16	Bloomington Stock Centre (USA)	BL#26263
w[1118]; P{y[+7.7] w[+mC]=GMR18H11-GAL4}attP2	Bloomington Stock Centre (USA)	BL#48832
w[1118]; P{y[+7.7] w[+mC]=GMR18H11-lexA}attP40	Bloomington Stock Centre (USA)	BL#52535
w[1118]; P{y[+7.7] w[+mC]=GMR92H07-GAL4}attP2	Bloomington Stock Centre (USA)	BL#40633

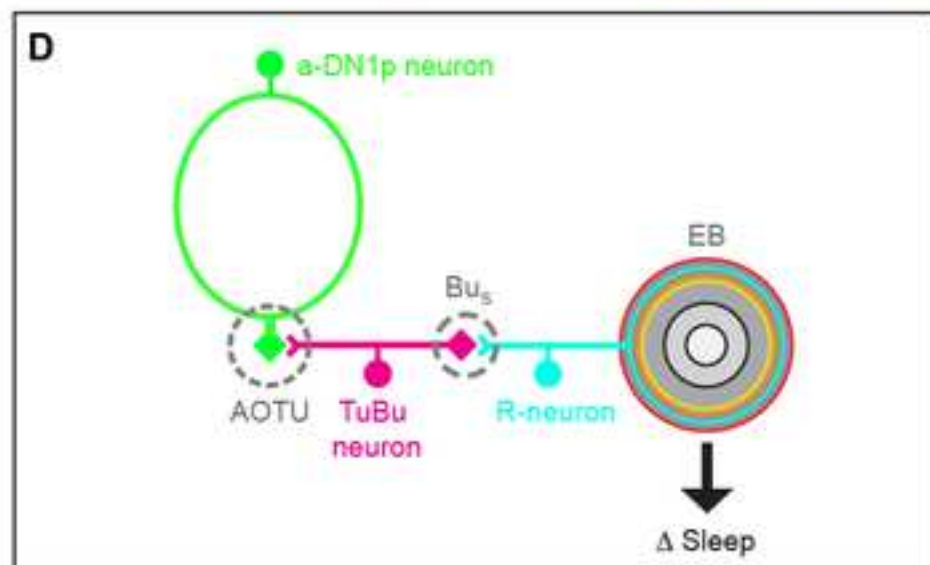
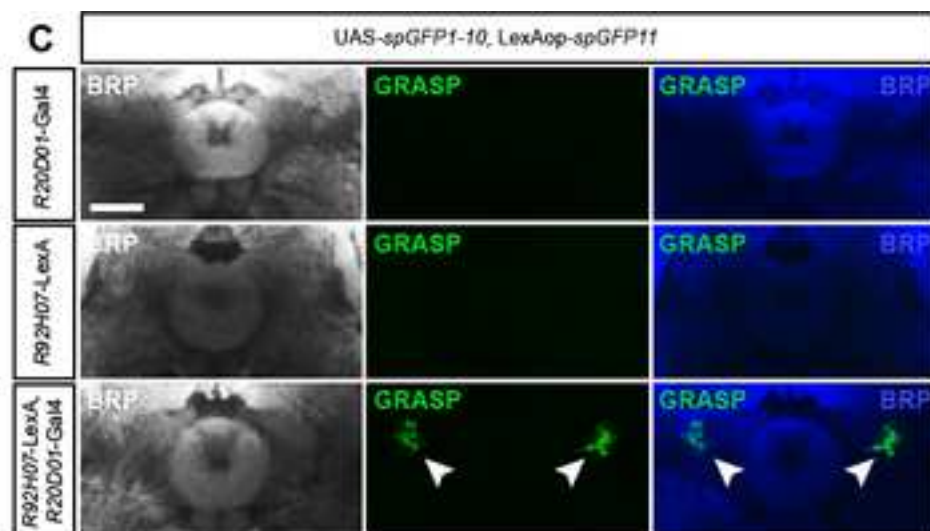
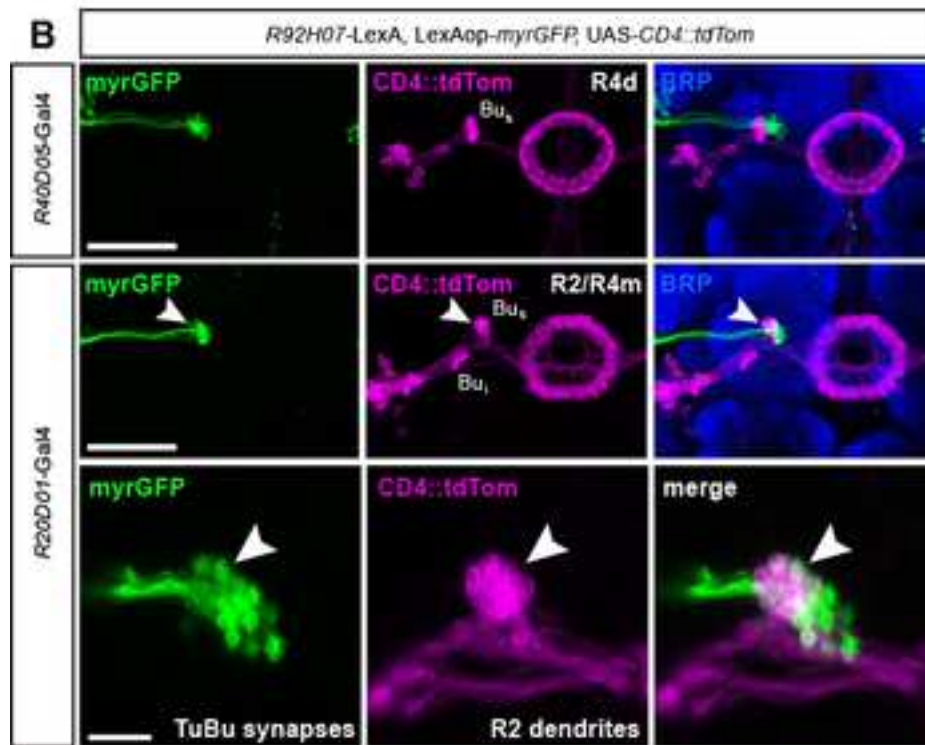
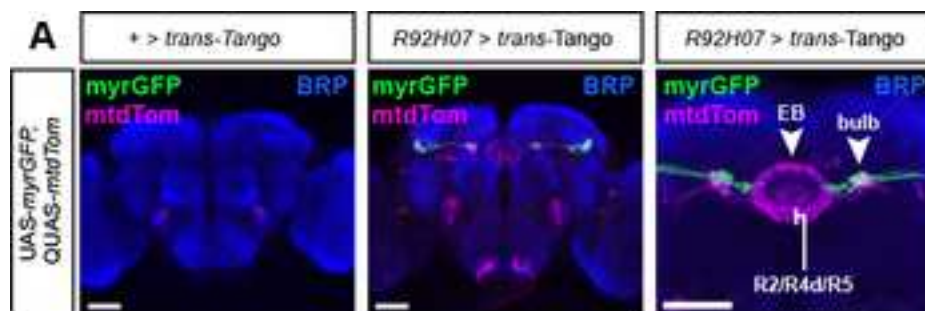
w[11118]; P{y[+t7.7] w[+mC]=GMR92H07-lexA}attP40/CyO	Bloomington Stock Centre (USA)	BL#54396
w[11118]; P{y[+t7.7] w[+mC]=GMR20D01-GAL4}attP2	Bloomington Stock Centre (USA)	BL#48889
w[11118]; P{y[+t7.7] w[+mC]=GMR40D05-GAL4}attP2	Bloomington Stock Centre (USA)	BL#50084
w[11118]; P{y[+t7.7] w[+mC]=GMR83H09-GAL4}attP2	Bloomington Stock Centre (USA)	BL#41311
w[*]; P{y[+t7.7] w[+mC]=UAS-CaMPARI.V398D}attP40	Bloomington Stock Centre (USA)	BL#58762
w[11118]; P{y[+t7.7] w[+mC]=13XLexAop2-IVS-GCaMP6s-SV40}su(Hw)attP1	Bloomington Stock Centre (USA)	BL#44273
y[1] w[11118]; PBac{y[+mDint2] w[+mC]=UAS-ChR2.XXL}VK00018	Bloomington Stock Centre (USA)	BL#58374
w[*]; P{w[+mC]=UAS-syt.eGFP}3	Bloomington Stock Centre (USA)	BL#6926
w[11118]; P{w[+mC]=UAS-DenMark}3	Bloomington Stock Centre (USA)	BL#33061
y[1] w[*]; P{w[+mC]=UAS-CD4-tdTom}7M1	Bloomington Stock Centre (USA)	BL#35841
w[*]; P{y[+t7.7] w[+mC]=13XLexAop2-IVS-myr::GFP}attP40	Bloomington Stock Centre (USA)	BL#32210
w[*]; sna[ <i>Sco</i> ]/CyO; P{w[+mC]=Clk4.1M-GAL4}3/TM6B, Tb[1]	Bloomington Stock Centre (USA)	BL#36316
w[*]; P{w[+mC]=UAS-spGFP1-10}	Prof. Kristen Scott (UC Berkeley) [42]	N/A
w[*]; P{w[+mC]=lexAop-CD4-spGFP11}	Prof. Kristen Scott (UC Berkeley) [42]	N/A
w[*]; P{w[+mC]=UAS- <i>trans</i> -Tango	Prof. Gilad Barnea (Brown University) [34]	N/A

w[*]; P{w[+mC]=hs-FLPm5}2/ln(2LR)Gla, wg[Gla-1] PPO1[Bc]; TM2/TM6B, Tb[1]	Bloomington Stock Centre (USA)	BL#35533
y[1] w[1118]; Pin[1]/CyO; P{w[+mC]=UAS(FRT.stop)mCD8-GFP.H}14, P{w[+mC]=UAS(FRT.stop)mCD8-GFP.H}21B	Bloomington Stock Centre (USA)	BL#30032
Software and Algorithms		
R-based sleep analysis software package	This paper	N/A
Image-J/Fiji	Fiji	N/A
Prism	Graphpad	N/A
Adobe Illustrator CS6	Adobe Systems	N/A
Adobe Photoshop	Adobe Systems	N/A









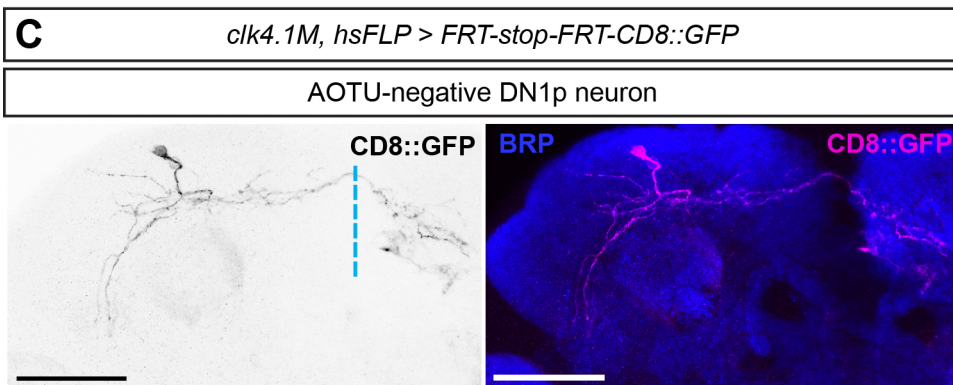
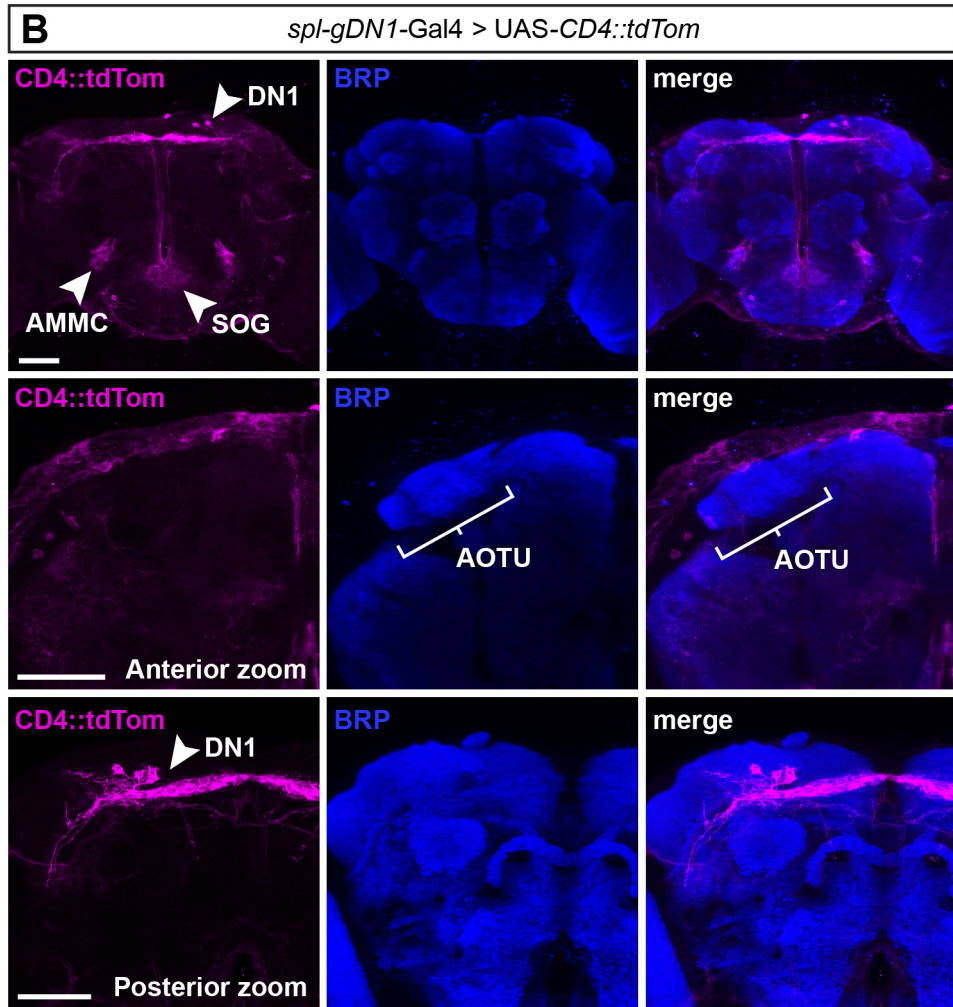
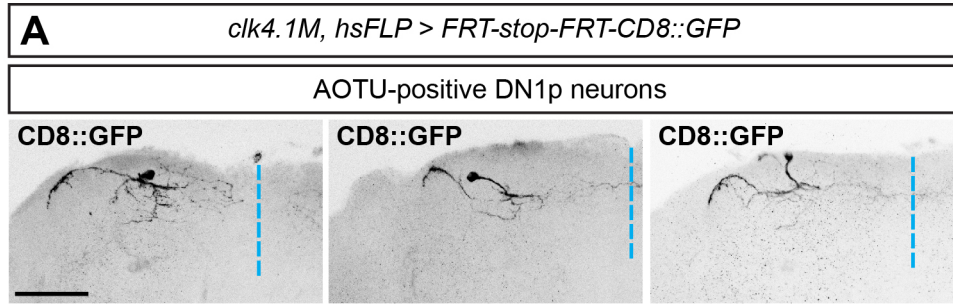


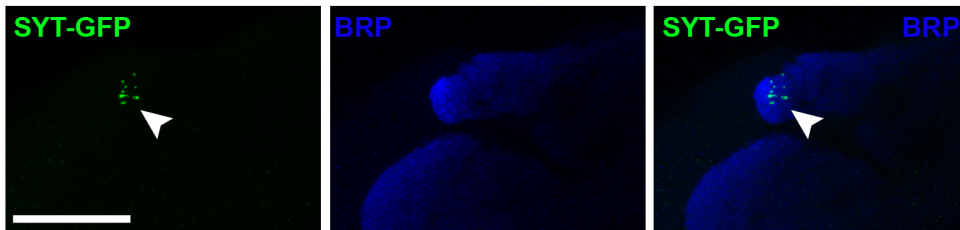
**Figure S1. AOTU-projecting DN1p (a-DN1p) neurons are not labelled by a DN1p-positive split-Gal4. Related to Figure 1.**

(A) Confocal z-stacks showing posterior cell bodies and projections of three individual DN1p neurons that innervate the Anterior Optic Tubercle (AOTU). Blue dotted lines denote the dorso-ventral midline of the *Drosophila* brain. Projections from one neuron (left panel) extend towards the midline but are confined to the ipsilateral domain. In contrast, fine projections from two other DN1p neurons (middle and right panels) extend past the midline into the contralateral domain. In each case the termination sites are close to the pars intercerebralis (PI), a known circadian output site [S1]. Scale bar, 20  $\mu\text{m}$ .

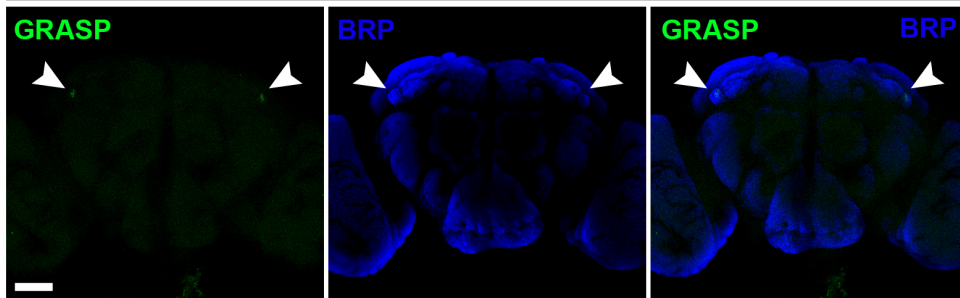
(B) Confocal z-stacks illustrating expression pattern of DN1p split-Gal4 (spl-gDN1) in the adult male *Drosophila* brain [S2], defined by expression of the membrane-tagged CD4::tdTomato (tdTom) fluorophore. Upper panels, anterior images of the *Drosophila* brain. tdTom fluorescence can be observed in dorsal projections (DN1 neurons) as well as in projections innervating the suboesophageal ganglion (SOG) and the antennal mechanosensory motor center (AMMC). Glial cells are also labelled. Presynaptic neuropil is labelled using an antibody against Bruchpilot (BRP). Middle panel, magnified view of the AOTU. tdTom driven by spl-gDN1-Gal4 was not detected in this neuropil domain. Lower panel: posterior projections of spl-gDN1 neurons. Scale bars: 50  $\mu\text{m}$ .

(C) Single mosaic DN1p neuron labelled with membrane-tagged CD8::GFP that does not innervate the AOTU. This DN1p neuron sends projections along to the posterior region to the contralateral domain, in close proximity to the PI. Note the similarity in projection patterns between this neuron and the collective spl-gDN1 population shown above. Blue dotted line denotes the dorso-ventral midline. Scale bars: 50  $\mu\text{m}$ .

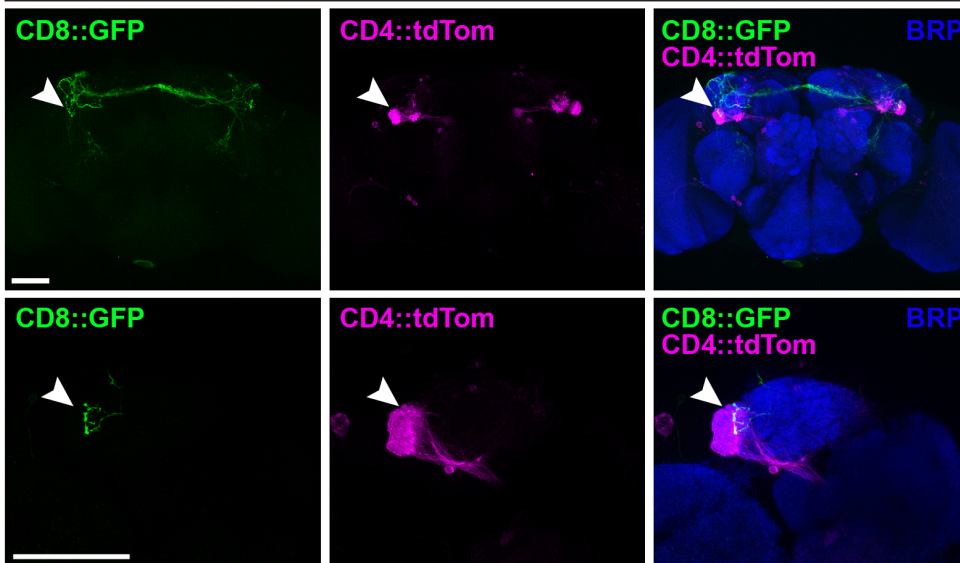
**A** *clk4.1M-Gal4 > UAS-syt-GFP*



**B** *R18H11-LexA > LexAop-spGFP11*  
*R92H07-Gal4 > UAS-spGFP1-10*



**C** *R18H11-LexA > LexAop-CD8::GFP*  
*R83H09-Gal4 > UAS-CD4::tdTom*



**D** *R18H11-LexA > LexAop-spGFP11*  
*R83H09-Gal4 > UAS-spGFP1-10*

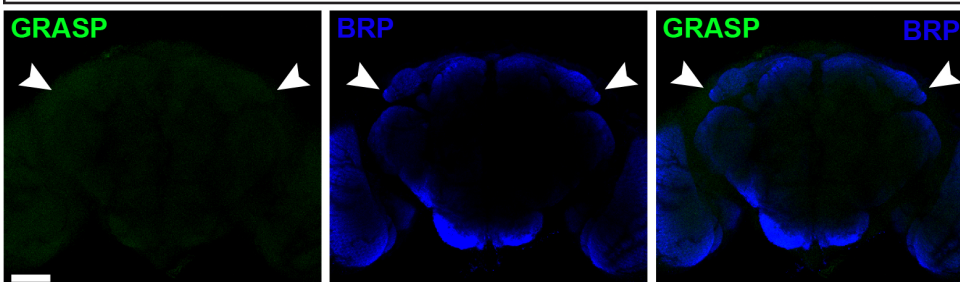


**Figure S2. DN1p neurons make synaptic connections with TuBu neurons in the AOTU. Related to Figure 2.**

(A) Confocal images showing localisation of presynaptic SYT-GFP in *clk4.1M*-Gal4-expressing adult male DN1p neurons. Arrows point to SYT-GFP puncta within the anterior optic tubercle (AOTU). BRP: Bruchpilot (a presynaptic neuropil marker).

(B) Confocal images showing that GRASP signal obtained through expression of split-GFP fragments in DN1p neurons (via *R18H11*-LexA) and TuBu neurons (via *R92H07*-Gal4) is detected specifically in the AOTU (arrows), and not elsewhere in the central brain.

(C) Dual labelling of DN1p and *R83H09*-positive TuBu neurons that innervate the lateral AOTU. Arrows point to DN1p presynaptic termini that tile the boundary of the lateral AOTU, and thus the dendritic domain of *R83H09*-TuBu neurons.

(D) Confocal images showing lack of GRASP signal from split-GFP fragments expressed in DN1p neurons (via *R18H11*-LexA) and *R83H09*-TuBu neurons. Arrows point to the AOTU region. No GRASP signal was detected in the AOTU or elsewhere in the *Drosophila* brain (compare with Figure S2A).

Scale bars: 50  $\mu$ m.

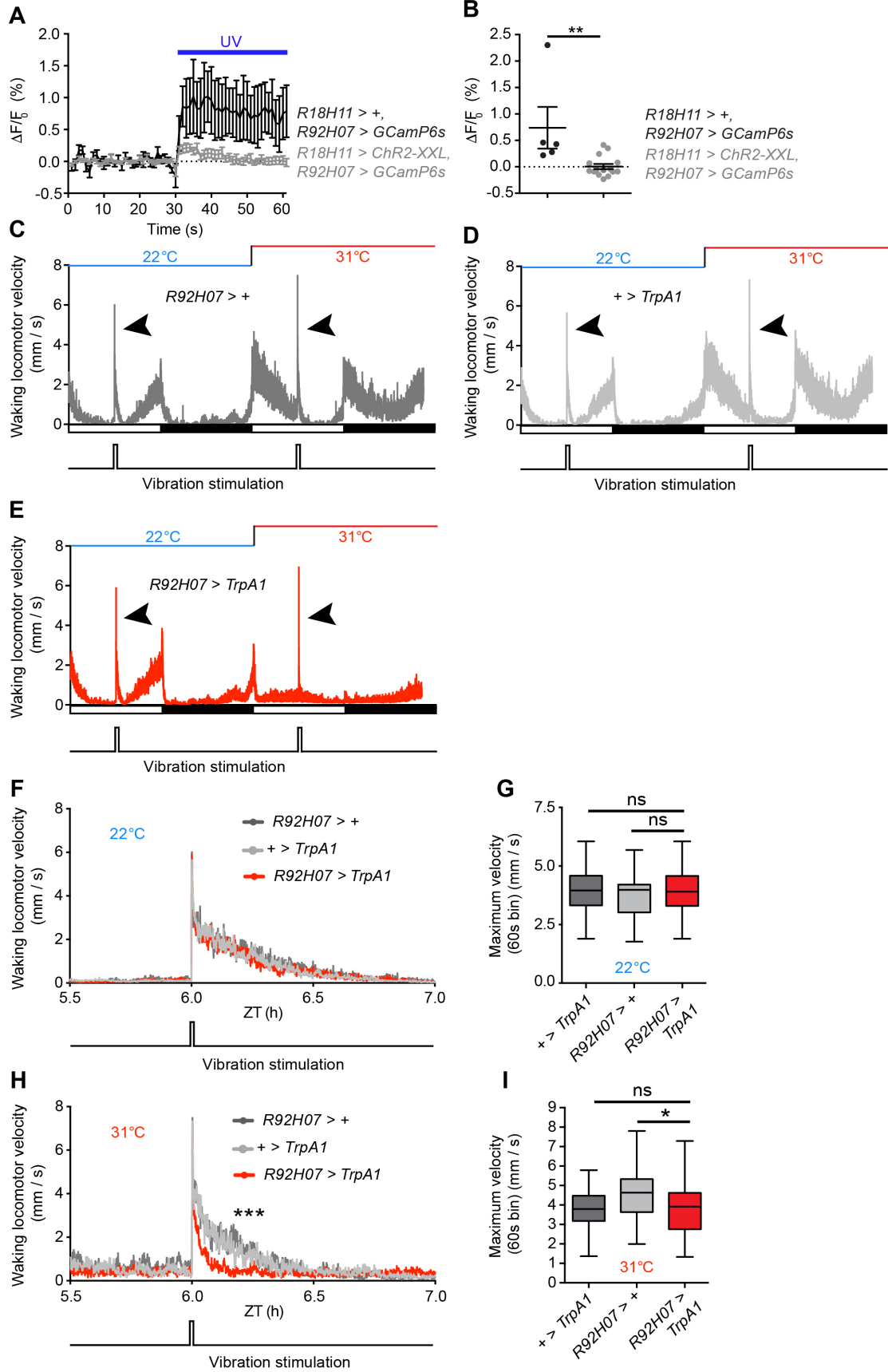


### Figure S3. Activation of *R92H07*-neurons does not cause paralysis.

#### Related to Figure 3.

(A) Mean change in GCaMP6s fluorescence in *R92H07*-TuBu neurons (*R92H07*-LexA > LexAop-GCaMP6s) following UV light activation of ChR2-XXL in DN1p neurons (grey; *R18H11*-Gal4 > UAS-*ChR2*-XXL), or solely due to UV light stimulation (black). Error bars represent SEM. Experiments were performed at ZT9, when DN1p excitability is normally low [S3]. In control brains expressing GCaMP6s in *R92H07*-TuBu neurons, excitation with UV light causes an increase in GCaMP6s fluorescence due to an overlap with the GCaMP6s excitation spectra. However, when UV light-activated ChR-XXL was simultaneously expressed in DN1p neurons, this increase in GCaMP6s fluorescence was reduced, indicative of a parallel reduction in intracellular calcium.

(B) Dot plots of individual cellular changes in GCaMP6s fluorescence following UV light stimulation in the presence (grey) or absence (black) of ChR2-XXL expressed in DN1p neurons. Mean and SEM are shown. \*\* $p < 0.01$ , Mann-Whitney U-test.

(C-E) Mean locomotor velocities in control (*R92H07* > +, C; + > *TrpA1*, D) and experimental adult male flies (*R92H07* > *TrpA1*, E), recorded using the DART video-tracking system [S4]. Control and experimental flies subjected to 24 h temperature shifts from 22°C to 31°C across two day/night cycles, where 22°C and 31°C are non-activating and activating temperatures for the *TrpA1* thermo-sensor respectively [S5]. DART was simultaneously used to apply mechanical vibration stimuli (noted below velocity graphs) to induce locomotor startle responses (arrows). Stimuli were applied at Zeitgeber Time (ZT) 6, when flies are normally quiescent. While activation of *R92H07*-neurons strongly suppressed spontaneous waking locomotor velocities (compare E with C, D during 31°C), robust startle responses to mechanical stimuli were still observed.

(F-I) Startle-induced locomotion at ZT6 in *R92H07* > *TrpA1* adult males or controls at either the non-activating condition (22°C, F-G) or the activating condition (31°C, H-I). Mean locomotor velocities before, during and after startle responses to mechanical stimuli are shown in (F, H). Median maximum locomotor velocities induced by mechanical stimuli are shown in (G, I). No difference in maximum locomotor velocities was observed before or after activation of *R92H07*-neurons (G, I). \* $p < 0.05$ , ns –  $p > 0.05$ , Kruskal-Wallis test with Dunn's post-hoc test. At 22°C, no significant difference in the decay of startle responses was observed in *R92H07* > *TrpA1* adult males compared to both controls (F).  $\tau^{\text{decay}}$  (h): *R92H07* > +, 0.2976; + > *TrpA1*, 0.2527; *R92H07* > *TrpA1*, 0.2587. + > *TrpA1* vs. *R92H07* > *TrpA1*,  $p = 0.486$ ; *R92H07* > + vs. *R92H07* > *TrpA1*,  $p < 0.001$ , extra sum of squares  $F$  test. At 31°C, a significant difference in the decay of startle responses was observed in *R92H07* > *TrpA1* adult males compared to both controls (H).  $\tau^{\text{decay}}$  (h): *R92H07* > +, 0.2308; + > *TrpA1*, 0.2191; *R92H07* > *TrpA1*, 0.06314. + > *TrpA1* vs. *R92H07* > *TrpA1*,  $p < 0.001$ ; *R92H07* > + vs. *R92H07* > *TrpA1*,  $p < 0.001$ . *R92H07* > +,  $n = 25$ ; + > *TrpA1*,  $n = 42$ ; *R92H07* > *TrpA1*,  $n = 42$ .

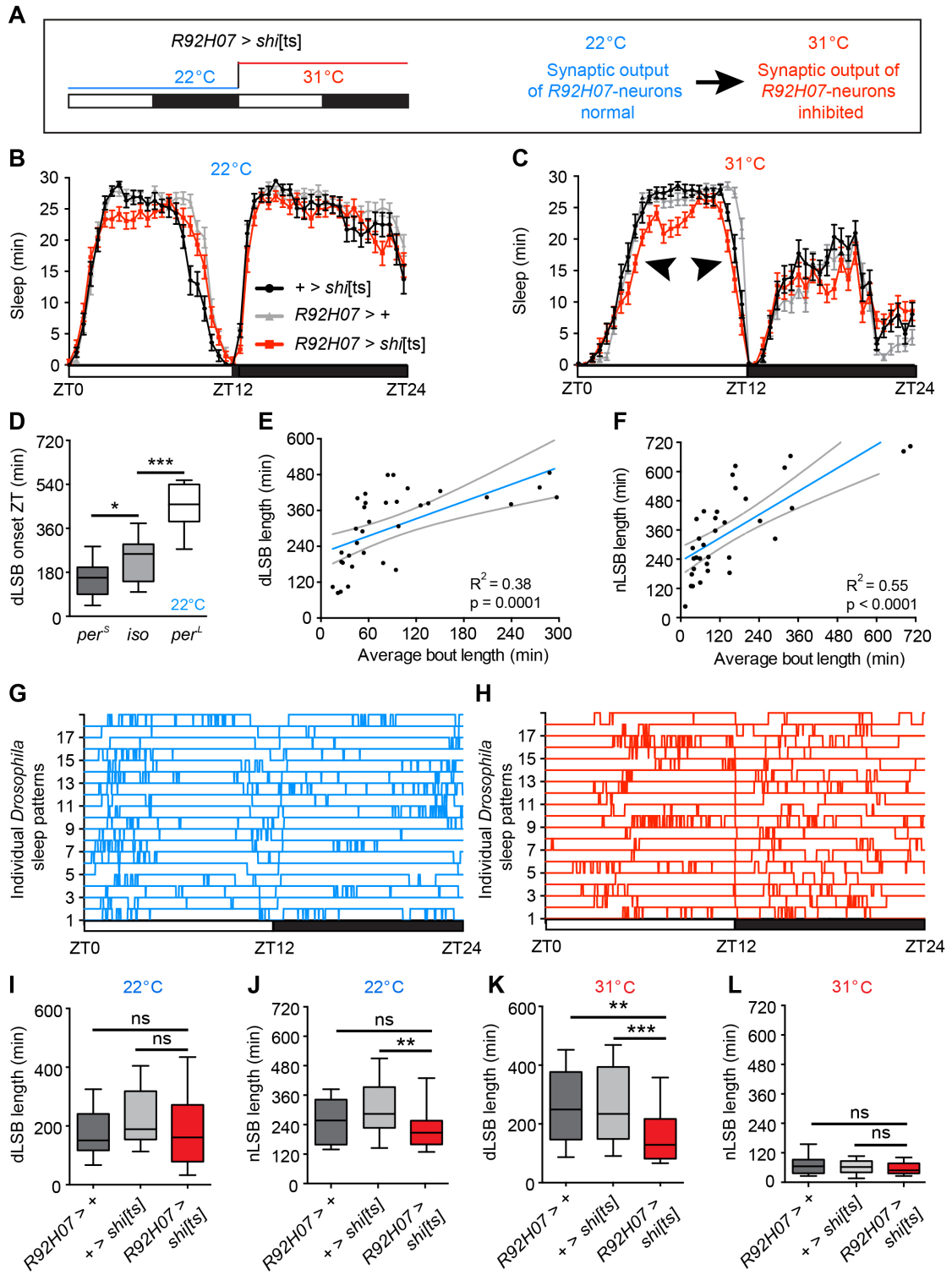


**Figure S4. Inhibition of *R92H07*-neurons reduces consolidated sleep during the day. Related to Figure 3.**

(A) Paradigm for acute inhibition of *R92H07*-neurons at elevated temperatures using *shi*[ts]. Light bars denote day, black bars denote night. (B-C) Mean sleep levels in adult male flies expressing *shi*[ts] in *R92H07*-neurons and controls, either at the non-inhibiting condition of 22°C (B) or the inhibiting condition of 31°C (C). Arrows point to the constriction of the domain of consolidated sleep following inhibition of *R92H07*-neurons. Error bars represent SEM. *R92H07* > +: n = 45; + > *shi*[ts]: n = 29; *R92H07* > *shi*[ts]: n = 41.

D) Onset of the daytime longest sleep bout (dLSB) in *iso31* control males, *per*<sup>S</sup> and *per*<sup>L</sup> mutants at 22°C. Tukey box plots show the 25<sup>th</sup>, median and 75<sup>th</sup> percentiles. Whiskers show 1.5x the interquartile range. *per*<sup>S</sup>: n = 30; *iso31*: n = 31; *per*<sup>L</sup>: n = 37.

(E, F) Correlation of the length of the longest and average sleep bouts during the day (E) or the night (F) in *iso31* male controls. dLSB: daytime longest sleep bout. nLSB: night time longest sleep bout. Blue lines, linear regression. Grey lines, 95% confidence intervals. R<sup>2</sup> and significance (p-value) from a slope of zero are shown. n = 34.

(G, H) Stacked binary sleep plots of n = 18 individual *iso31* control males at either 22°C (G) or 31°C (H). Down-states represent movement (i.e non-sleep), up-states represent sleep. Note several time-windows in which sleep becomes highly fragmented, including the morning at 22°C (G) and a substantial portion of the night at 31°C (H).

(I-L) Inhibition of *R92H07*-neurons reduces the duration of consolidated sleep during the day. At the permissive temperature of 22°C, the length of the longest day (dLSB) and night (nLSB) sleep bouts were unaffected by expression of *shi*[ts] (I, J). At 31°C, inhibition of synaptic release from *R92H07*-neurons results in a significant reduction in length of the dLSB (K) but not the nLSB (L). \*\*p < 0.01, \*\*\*p < 0.001, ns – p > 0.05, Kruskal-Wallis test with Dunn's post-hoc test. *R92H07* > +: n = 45; + > *shi*[ts]: n = 29; *R92H07* > *shi*[ts]: n = 41.

## Supplemental references

- S1. Cavanaugh, D.J., Geratowski, J.D., Wooltorton, J.R., Spaethling, J.M., Hector, C.E., Zheng, X., Johnson, E.C., Eberwine, J.H., and Sehgal, A. (2014). Identification of a circadian output circuit for rest:activity rhythms in *Drosophila*. *Cell* *157*, 689-701.
- S2. Guo, F., Chen, X., and Rosbash, M. (2017). Temporal calcium profiling of specific circadian neurons in freely moving flies. *Proc Natl Acad Sci U S A* *114*, E8780-E8787.
- S3. Flourakis, M., Kula-Eversole, E., Hutchison, A.L., Han, T.H., Aranda, K., Moose, D.L., White, K.P., Dinner, A.R., Lear, B.C., Ren, D., et al. (2015). A Conserved Bicycle Model for Circadian Clock Control of Membrane Excitability. *Cell* *162*, 836-848.
- S4. Faville, R., Kottler, B., Goodhill, G.J., Shaw, P.J., and van Swinderen, B. (2015). How deeply does your mutant sleep? Probing arousal to better understand sleep defects in *Drosophila*. *Sci Rep* *5*, 8454.
- S5. Hamada, F.N., Rosenzweig, M., Kang, K., Pulver, S.R., Ghezzi, A., Jegla, T.J., and Garrity, P.A. (2008). An internal thermal sensor controlling temperature preference in *Drosophila*. *Nature* *454*, 217-220.